

Crack healing of alumina according to the added amount of silicon carbide

Kwang-Ho Lee^a, Ki-Woo Nam^b and Seok-Hwan Ahn^{c,*}

^aDaewoo Shipbuilding & Marine Engineering Co., Ltd., Gyeongsangnam-do, 53302, Korea

^bDepartment of Materials Science and Engineering, Pukyong National University, Busan 48547, Korea

^cDepartment of Mechatronics, Jungwon University, Chungbuk, 28024, Korea

Three kinds of Al₂O₃-composite ceramic were prepared using mixtures of Al₂O₃, SiC and Y₂O₃. The Y₂O₃ was set as constant to 3 wt%, while three concentrations of the silicon carbide were applied (10, 15, and 20 wt%). The crack healing was studied as functions of the heat-treatment temperature and the amount of SiC. The heat treatment was carried out at 1473, 1573, and 1673 K for 1 hr in air. The results show that the corresponding crack-healing ability is superior regardless of the added amount of SiC.

Key words: Al₂O₃, concentration of SiC, Y₂O₃, Vickers Indentation, Crack Healing.

Introduction

Alumina (Al₂O₃) is the most common ceramic material, and it has been used in a variety of applications such as various protection tubes, cutting tools, grindstones, and electronic boards through the utilization of heat resistance, corrosion resistance, abrasion resistance, and electric insulation. Due to the brittleness and low toughness of ceramics, however, their reliability is low and their use is limited to critical appliances. A general method of overcoming the brittleness of ceramics, known as a toughness improvement, is the method of compounding the ceramic particles of micro or submicro sizes or the whiskers [1-3]. Recently, silicon carbide (SiC) has been mixed to impart a crack-healing ability, thereby improving the strength of ceramics [4-7]. The conclusion of the researchers of this SiC study is that the oxidation product is an important factor of the crack healing [8-13]. From this perspective, researchers are actively studying the self-healing ability of structural ceramics, which play a leading role on the global scale [14-18]. The mechanical properties of those structural ceramics with a self-crack-healing ability are superior to those of the base materials.

In this study, the crack-healing phenomenon of Al₂O₃ was investigated according to the constant addition of 3-wt% yttria (Y₂O₃) and the changing of the added SiC to 10, 15 and 20 wt% concentrations, both of which facilitate the crack-healing ability. In addition, the healing strengths of long cracks were compared.

Materials and Experimental Method

The commercially available Al₂O₃ (AA-04, Sumitomo Chemical, Japan), ultrafine-grade SiC (Ibiden, Japan), and Y₂O₃ (Nippon Yttrium, Japan) were used as the starting materials. The mean particle size of the Al₂O₃ is 0.5 μm, and those of the SiC and Y₂O₃ powders are both 0.27 μm. To evaluate the crack-healing properties, the SiC was respectively added at the 10, 15, and 20 wt% concentrations. The Y₂O₃ was added at the concentration of 3 wt%. Hereinafter, the three kinds of specimens were called AS10Y3, AS15Y3, and AS20Y3, respectively. The mixtures were milled in isopropanol for 24 hrs using an Al₂O₃ ball (φ5), followed by their placement in a 363 K furnace to extract the solvent, and to make the dry-powder mixtures. The dry powder was then passed through a 106 μm sieve. The mixtures were subsequently hot-pressed in nitrogen gas (N₂) for 1 hr via a hot pressing that was conducted under 35 MPa at 1873 K. Table 1 shows each composition, and Fig. 1 shows the sintering flowchart.

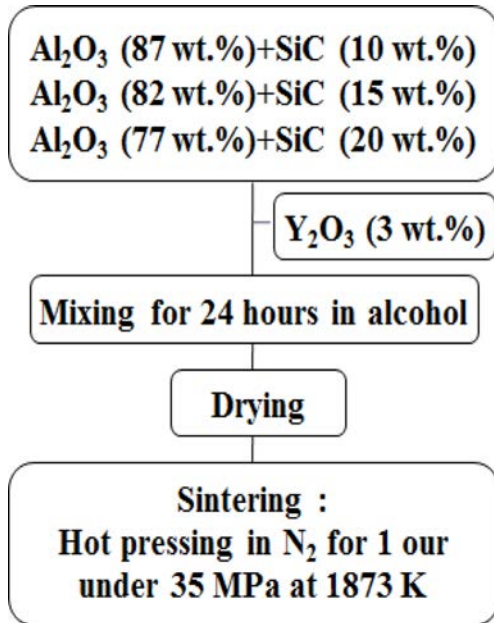
The hot-pressed materials were also machined to produce bar specimens of the dimensions 3 × 4 × 18 mm, and these were polished and beveled to reduce the likelihood of edge-initiated failures. The specimens, with a span length of 16 mm, were made according to the Japanese Industrial Standards (JIS). A Vickers-indentation precrack was made in the center of the polished face of the bar specimen at the loads of 19.6, 49, 98, and 196 N in air. A long crack was made by a multiple indentation with the indentation load of 19.6 N.

The crack-healing condition exerted a large effect on the fracture strength. The crack-healing time was at 1473, 1573, and 1673 K in air is 1 hr. The long-crack healing was carried out at 1573 K for 1 hr in air. The furnace was then used for a spontaneous cooling, and

*Corresponding author:
Tel : +82-43-830-8942
Fax: +82-43-830-8114
E-mail: shahn@jwu.ac.kr

Table 1. Batch composition of Al₂O₃/SiC composite ceramics.

Powder	Al ₂ O ₃ (wt.%)	SiC (wt.%)	Y ₂ O ₃ (wt.%)
AS10Y3	87	10	3
AS15Y3	82	15	3
AS20Y3	77	20	3

**Fig. 1.** Flow chart of sintering.

the crack-healing specimen was subsequently tested in a three-point bending at a crosshead speed of 0.5 mm/min using a fixture with a span of 16 mm.

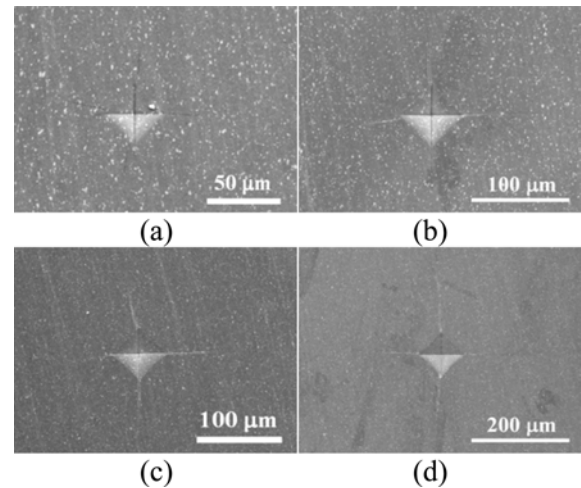
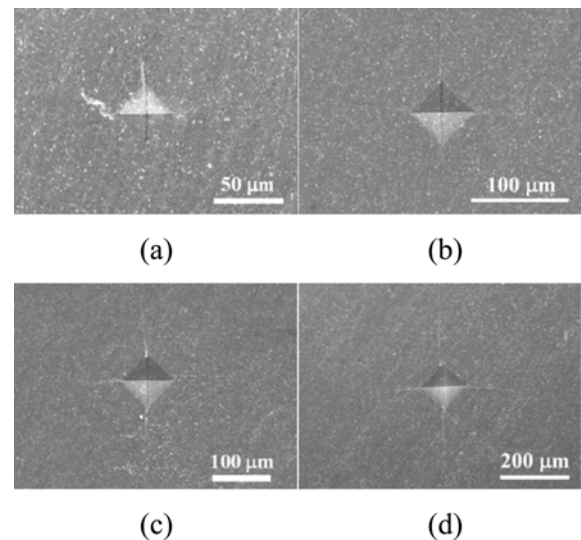
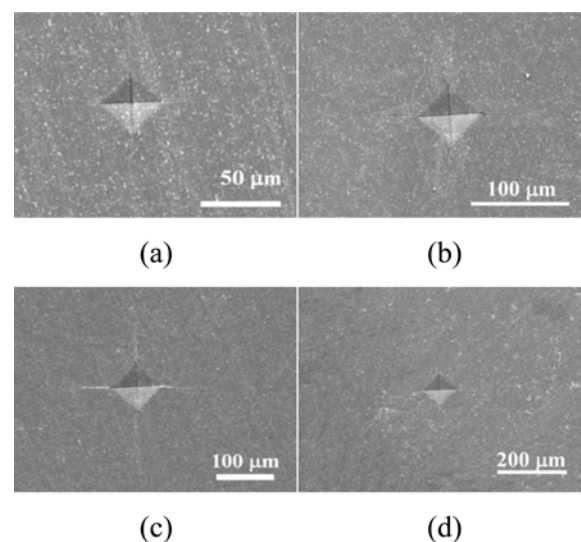
The before- and after- crack-healing and the fracture surface were observed using scanning electron microscopy (SEM). The components of the healing part were line-profiled using energy-dispersive X-ray spectroscopy (EDX). The specimen composition regarding the heat-treatment time and temperature was analyzed using X-ray diffraction (XRD).

Results and Discussion

Crack length due to the indentation load

Figs. 2-4 show the crack growth of the three specimens according to the Vickers-indentation loads of 19.6, 49, 98, and 196 N. The AS10Y3, AS15Y3, and AS20Y3 specimens are shown in Figs. 2, 3, and 4, respectively. The Vickers-indentation shapes of each specimen are distinct, thereby revealing the cracks that were grown at the Vickers-indentation edge. It is evident that the cracks grew with the increasing of the load regardless of the specimen.

Fig. 5 shows the crack length of the three specimens according to the Vickers-indentation load. The crack length represents the length at the center of the Vickers indentation, and the crack growth increased as the

**Fig. 2.** Crack appearance according to indentation load in AS10Y3. (a) 19.6 N, (b) 49 N, (c) 98 N, (d) 196 N.**Fig. 3.** Crack appearance according to indentation load in AS15Y3. (a) 19.6 N, (b) 49 N, (c) 98 N, (d) 196 N.**Fig. 4.** Crack appearance according to indentation load in AS20Y3. (a) 19.6 N, (b) 49 N, (c) 98 N, (d) 196 N.

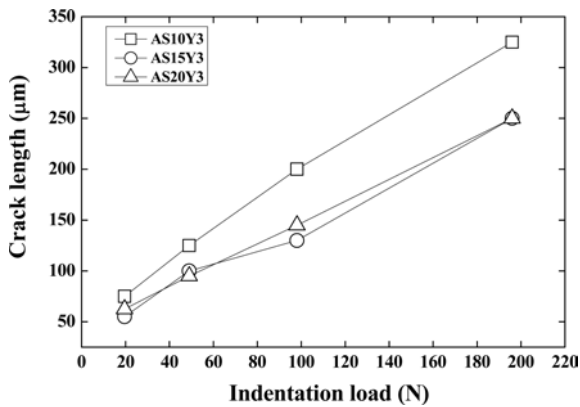
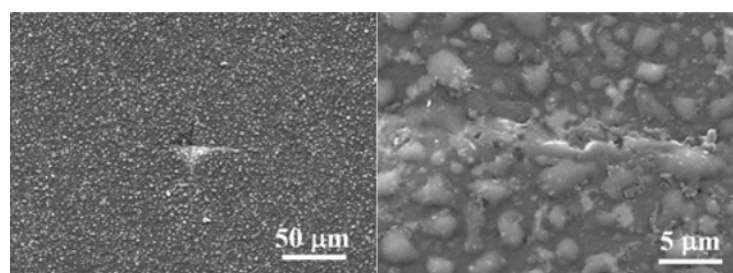


Fig. 5. crack length according to indentation load.

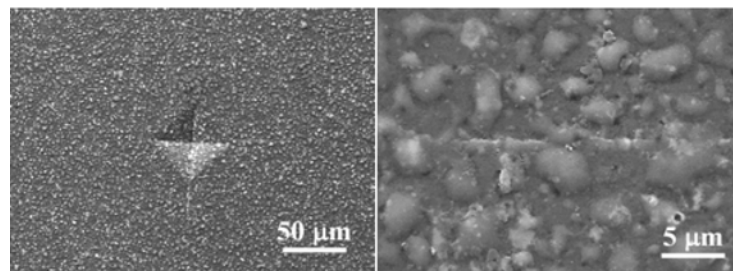
indentation load was increased. The crack length and SiC content of AS10Y3 are the longest and smallest, respectively, while the AS15Y3 and AS20Y3 specimens showed an almost-similar crack growth; this is because the strength of Al_2O_3 is weaker than that of SiC, so the crack growth of the AS10Y3 specimen with the least SiC amount is large. When the added SiC quantity was increased to some extent, however, a similar strength and a similar crack growth were exhibited.

Crack healing by heat treatment

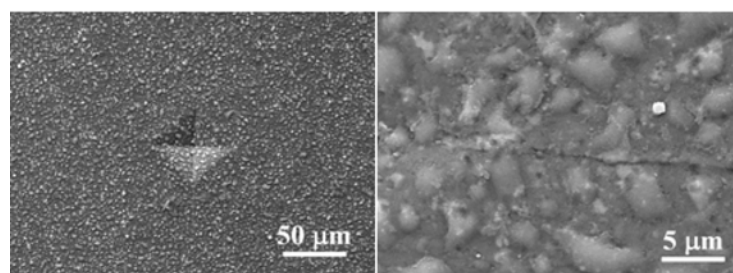
Figs. 6-11 show the crack-healing appearance of the three specimens. Figs. 6, 7, and 8 are the heat-treated AS10Y3, AS15Y3, and AS20Y3 specimens at 1473 K,



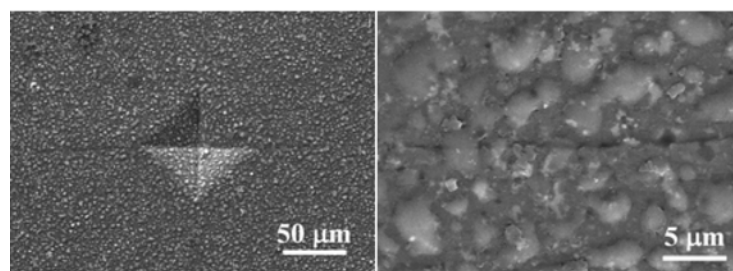
(a)



(b)



(c)



(d)

Fig. 6. Crack-healed appearance under 1 hr of 1473K in AS10Y3. (a) 19.6 N, (b) 49 N, (c) 98 N, (d) 196 N.

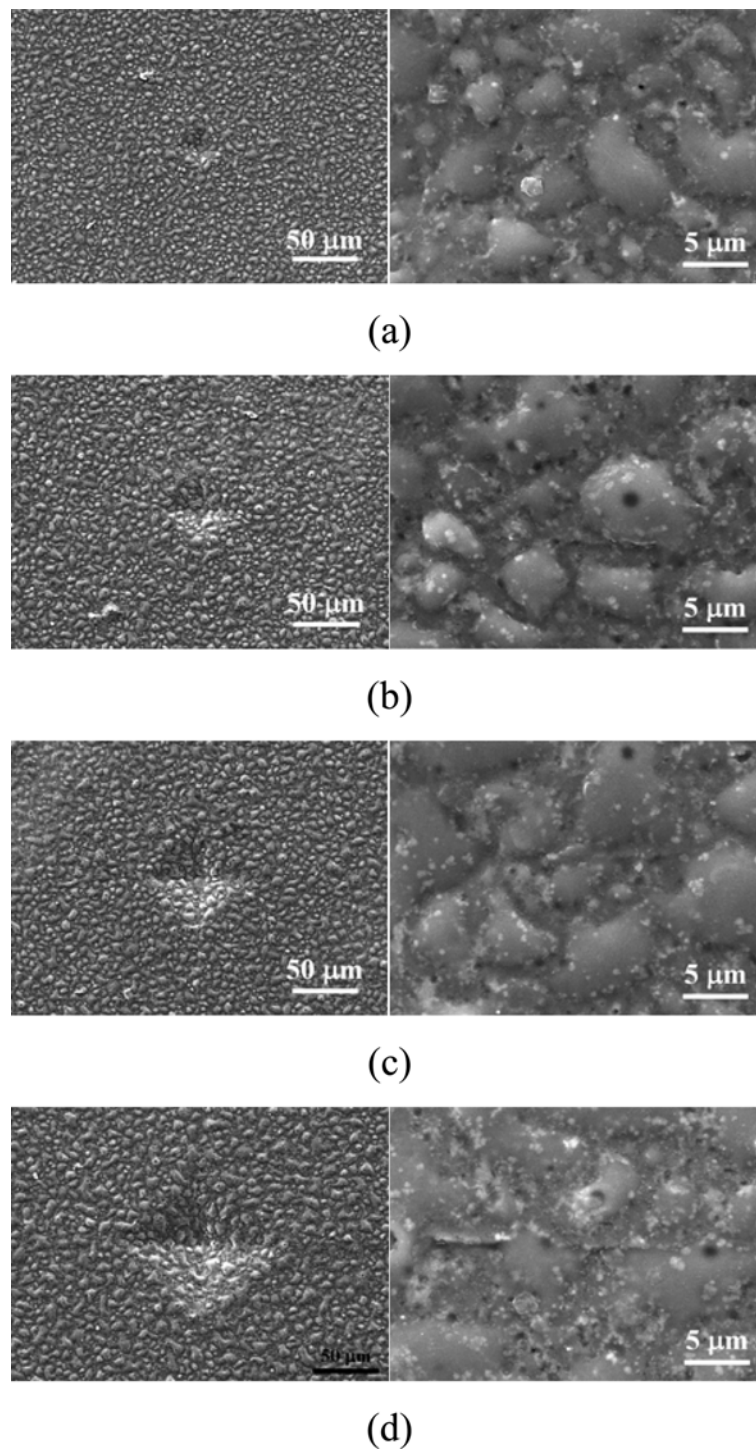


Fig. 7. Crack-healed appearance under 1 hr of 1473 K in AS15Y3. (a) 19.6 N, (b) 49 N, (c) 98 N, (d) 196 N.

respectively. Figs. 9 and 10 are the heat-treated AS15Y3 and AS20Y3 specimens at 1573 K, respectively. Fig. 11 is the heat-treated AS10Y3 specimen at 1673 K.

In Figs. 6-8, the indentation shape is retained. Here, a crack with a large indentation load is judged as incompletely healed; however, these cracks showed a higher strength than the bending strength of the smooth specimen, as described later, and a complete healing was finally identified. Further, if the SiC content of any

of the specimens is high, the indentation shape was reduced. The enlarged image shows that the lump shapes increased due to the flow phenomenon during the healing process.

In Figs. 9 and 10, a complete crack healing is displayed, unlike the specimens of the 1473 K heat treatment. In particular, the indentations that were caused by the load of 19.6 N can be observed dimly, but cracks could not be found. The surface lumps are

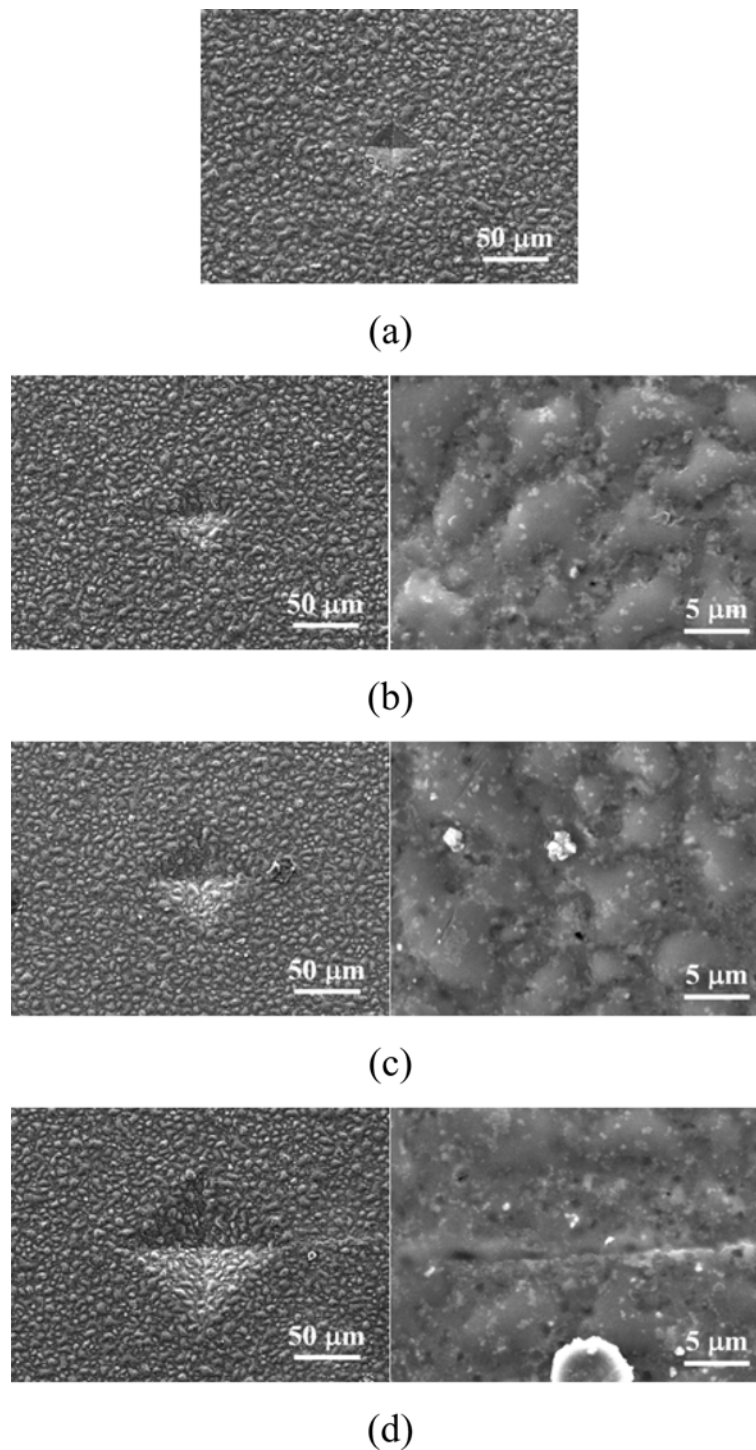


Fig. 8. Crack-healed appearance under 1 hr of 1473 K in AS20Y3. (a) 19.6 N, (b) 49 N, (c) 98 N, (d) 196 N.

like those of the 1473 K specimens, but they are low. In the enlarged image, the lumps are flatter than those of the 1473 K specimens and pores are evident in the lump parts. At the high temperatures, an oxidation reaction of the SiC-containing ceramic led to the formation of silicon dioxide (SiO_2), thereby healing the cracks.

Fig. 11 is the crack part of the AS10Y3 specimen that was caused by the load of 98 N and the healing at

1673 K. The visibility of the indentation is dim, but cracks are not evident. In the enlarged image, lumps are absent due to the pores and the flow phenomenon that are like those of the 1573 K specimens. With the exception of AS10Y3, cracks and indentations are not evident in the other specimens due to an excessive flow phenomenon.

Based on the surface observations, the cracks of the three specimens were healed by the heat treatment. To

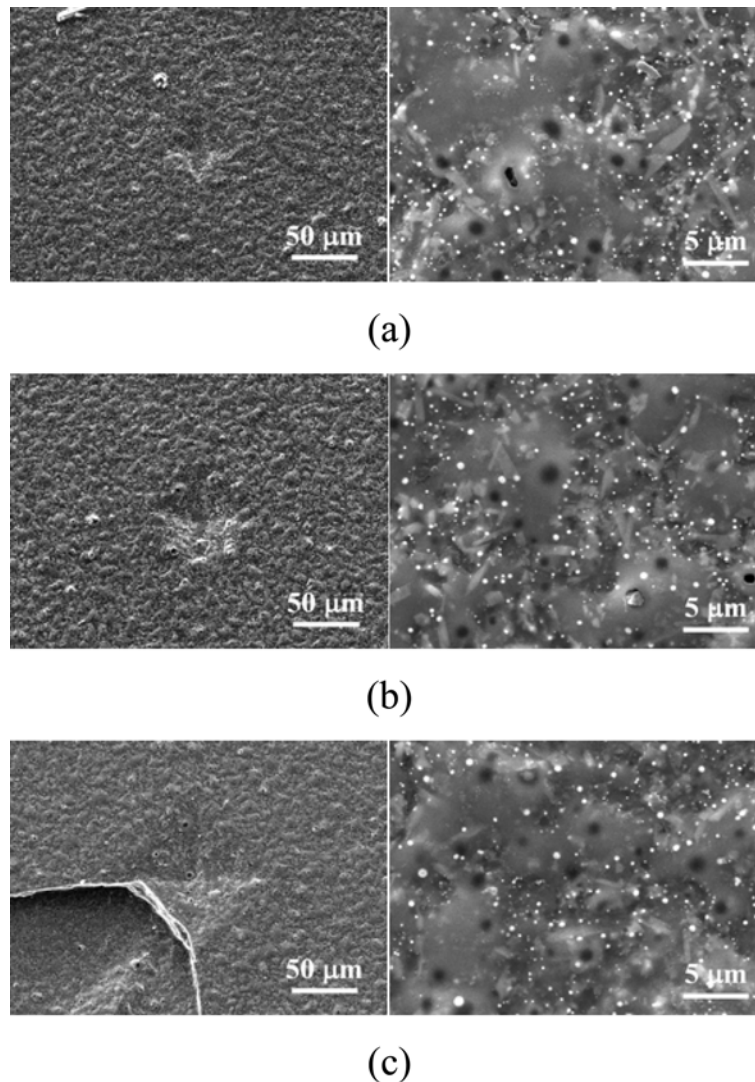


Fig. 9. Crack-healed appearance under 1 hr of 1573 K in AS15Y3. (a) 49 N, (b) 98 N, (c) 196 N.

confirm this, the crack specimen and the 1473 K healing specimens were subjected to an EDX line-profile analysis, and the results are shown in Fig. 12. Figs. 12(a), (b), and (c) display the AS10Y3, AS15Y3, and AS20Y3 specimens, respectively. It can be seen that the silicon (Si) and oxygen (O) amounts in the crack part of the crack specimen are low regardless of the SiC composition. The amounts of Si and O were increased in the crack-healing specimen, and they were increased as the temperature was increased. Alternatively, as the amount of SiC was increased, the amounts of Si and O in the healing area increased. Accordingly, it can be seen that the Si and O contributed to the crack healing.

SiO₂ consists of the following two phases: a glass phase and a crystalline phase. To investigate the crack-healing phase of SiO₂, an XRD analysis was performed according to the healing time using a specimen that was heat-treated at 1573 K. The results of this analysis are shown in Figs. 13-15, where, in each figure, (a) is a

smooth specimen, (b) is a heat-treatment specimen of 0.5 hr, (c) is a heat-treatment specimen of 1 hr, and (d) is a heat-treatment specimen of 10 hrs.

Fig. 13 shows the AS10Y3 specimen, where (a) presents the formation of the compound of a smooth specimen for which Y₂O₃ served as a sintering aid and Al₂O₃ was also used, but the SiC was not decomposed because of the lack of a healing treatment, and SiO₂ was not formed. In (b), the formation of the compound of the 0.5 hr heat-treatment specimen for which Y₂O₃ served as a sintering aid and Al₂O₃ was also used is presented, and Al₅Y₃O₁₂ represents a phase change from “trietrium pentaaluminium oxide” to “aluminum yttrium oxide”; however, the SiO₂ component was not detected for the 0.5 hr heat-treatment specimen. In (c), the detection of the aluminum (Al)-yttrium (Y) compound (Al₃Y) of the 1 hr heat-treatment specimen, which comprises a combination of Al and Y, is shown. As the heat-treatment time was extended, the SiC reacted with the O, forming SiO₂. The SiC phase

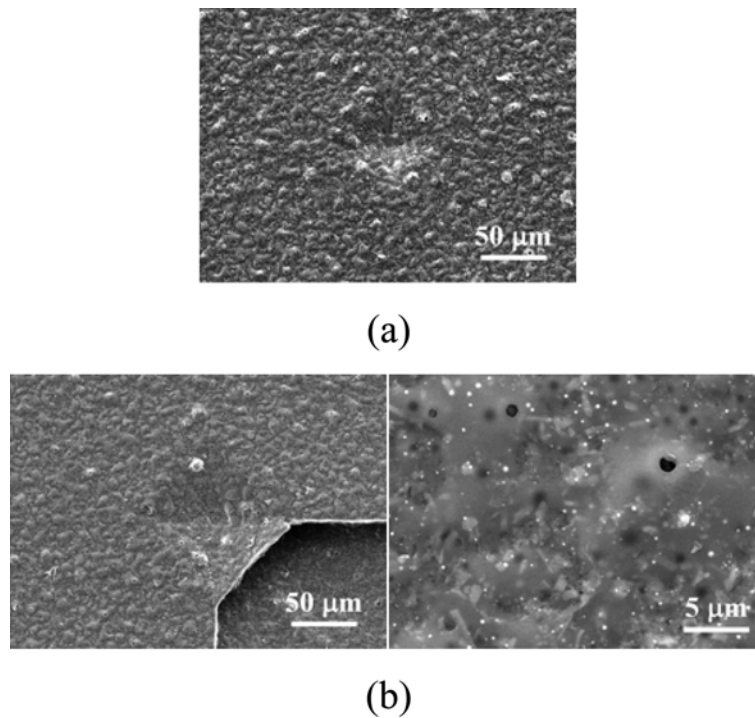


Fig. 10. Crack-healed appearance under 1 hr of 1573 K in AS20Y3. (a) 98 N, (b) 196 N.

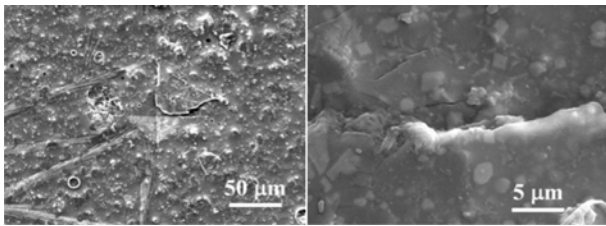


Fig. 11. Crack-healed appearance under 1 hr of 1673 K in AS10Y3 by 98 N.

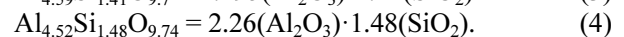
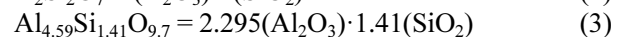
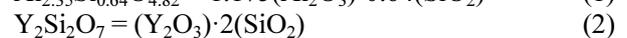
changed from “moissanite 3C” to “silicon carbide.” The compound $Y_2Si_2O_7$ that was produced by the reaction of the Y_2O_3 , O, and SiC was detected from the 10 hrs heat-treatment specimen. The entirety of the SiC was not converted to SiO_2 , and some of the SiC was detected as the “moissanite-36H” phase, which is different from the detected phase of the 1 hr heat-treatment specimen.

Fig. 14 shows the AS15Y3 specimen. Fig. 16(a) shows a phenomenon such as the AS10Y3 specimen. In (b), The 0.5 hr heat-treatment specimen was formed a compound by the Y_2O_3 served as a sintering aid and the Al_2O_3 ; here, the detected components and phase types are not different from those of the smooth specimen. In (c), the formed compound of the 1 hr heat-treatment specimen for which Y_2O_3 served as a sintering aid and Al_2O_3 was also used is displayed; as the heat-treatment time was extended, a mullite-type Al_2O_3 and SiO_2 compounds were detected in addition to SiO_2 . In (d), the detection of the Y_2O_3 of the 10 hr heat-treatment specimen is shown, but Y_2O_3 was not detected in the smooth specimen or the 0.5 and 1 hr heat-treatment specimens. In addition to SiO_2 , a

component of the mullite-type Al_2O_3 and SiO_2 was also detected. In spite of a sufficient 10 hr heating time, all of the SiC was not chemically changed to SiO_2 . The SiO_2 changed from “quartz low” to “silicon oxide.”

Fig. 15 shows the AS20Y3 specimen, where (a) shows a phenomenon such as the AS10Y3 and AS15Y3 specimens. In (b), a phenomenon such as the AS10Y3 specimen is displayed. In (c), of the 1 hr heat-treatment specimen was detected the SiO_2 , and sillimanite compound of Al and SiO_2 , while YH_2 , a compound of yttria (Y) and hydrogen (H), was also detected for this specimen. SiC was not detected and Si was detected in the form of other compounds. In (d), the 10 hr heat-treatment specimen wasn't detected SiC, while Si was detected in the form of another compound; furthermore, a compound with a “keiviite-(Y)” structure, in which Y_2O_3 and two SiO_2 are combined was detected. This was the compound composition of the mullite-type Al_2O_3 and SiO_2 .

Regarding the previous described figures, the 1 hr heat-treatment specimen at 1573 K formed SiO_2 . After the formation of the SiO_2 , it remained in an unchanged state without a reaction, or it existed in the form of a compound after a reaction with Al_2O_3 or Y_2O_3 , as follows:



However, the 10 hr heat-treatment specimen formed the Y_2O_3 - SiO_2 compound in the 10 wt% SiC. In the

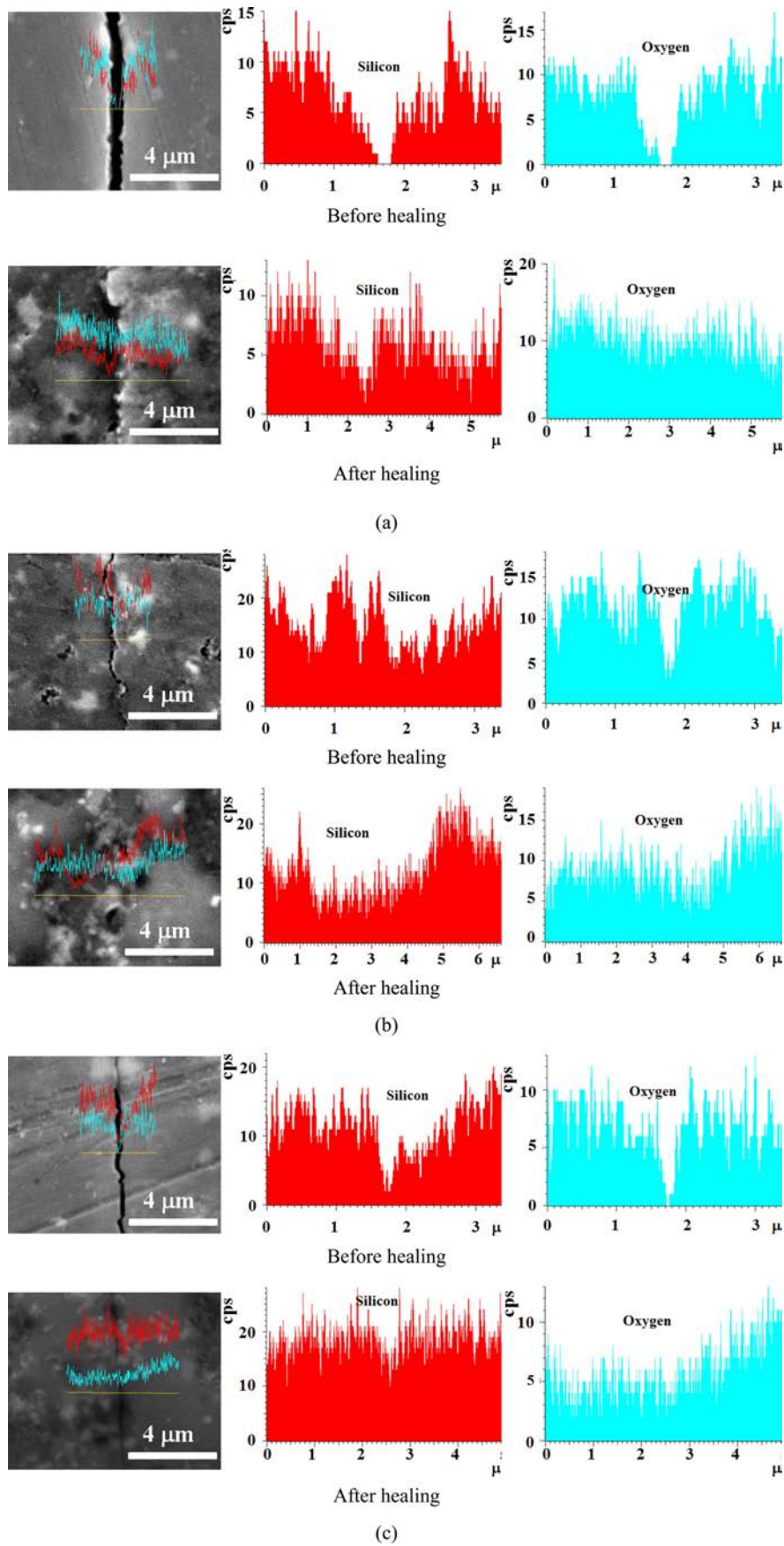


Fig. 12. Line profile for specimens of before and after crack healing. (a) AS10Y3, (b) AS15Y3, (c) AS20Y3.

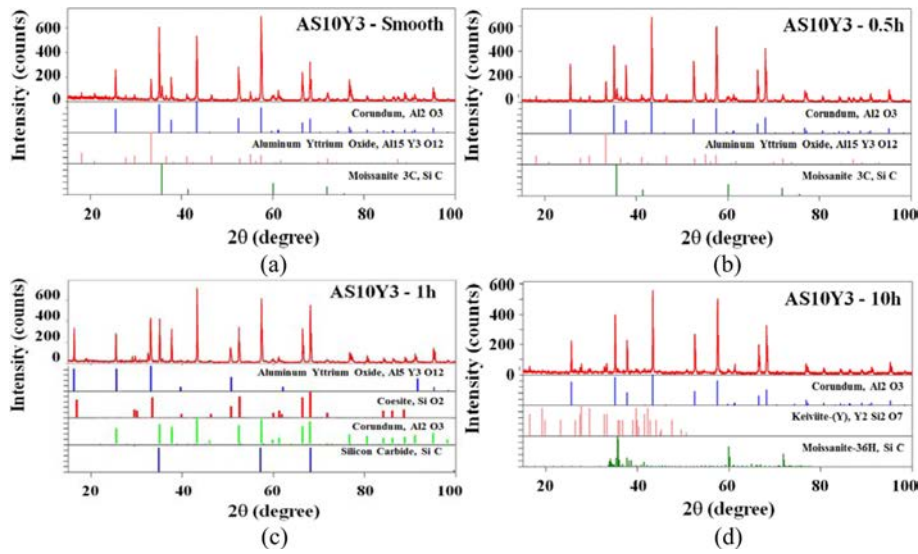


Fig. 13. XRD analysis according to healing time in AS10Y3. (a) 0 hr, (b) 0.5 hr, (c) 1 hr, (d) 10 hr.

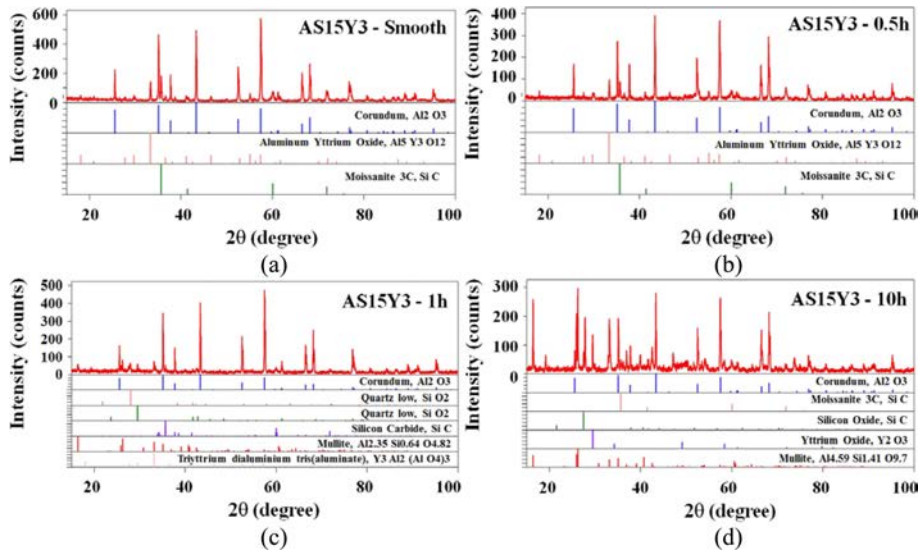
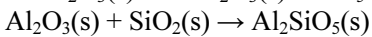
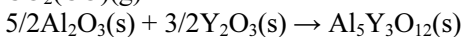
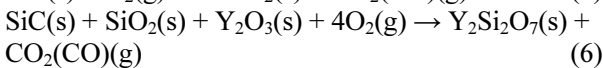
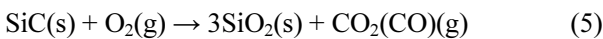


Fig. 14. XRD analysis according to healing time in AS15Y3. (a) 0 hr, (b) 0.5 hr, (c) 1 hr, (d) 10 hr.

15 wt% SiC, an $\text{Al}_2\text{O}_3\text{-SiO}_2$ compound was formed, and in the 20 wt% SiC, $\text{Y}_2\text{O}_3\text{-SiO}_2$ and compounds were formed. The healing reaction of the heat-treatment specimen is as follows:



Bending strength at room temperature

Fig. 16 shows the effects of the SiC content on the bending strength and the crack-healing behavior. The square symbols (\square , \blacksquare) indicate AS10Y3, the circle symbols (\circ , \bullet) indicate AS15Y3, and the triangular symbols (Δ , \blacktriangle) indicate AS20Y3. Table 2 shows the

Table 2. Bending strength of $\text{Al}_2\text{O}_3/\text{SiC}$ composite ceramics.

	AS10Y3 (MPa)	AS15Y3 (MPa)	AS20Y3 (MPa)
Smooth	472.0 ± 35.81	497.0 ± 33.36	520.3 ± 38.16
Healing smooth at 1573 K	824.6 ± 19.63	894.9 ± 48.59	882.6 ± 45.83
Crack	219.0 ± 35.95	221.3 ± 18.89	240.3 ± 11.46
Healing crack at 1473 K	753.1 ± 31.40	694.4 ± 17.23	755.3 ± 27.72
Healing crack at 1573 K	798.2 ± 61.49	765.5 ± 54.90	802.3 ± 66.31
Healing crack at 1673 K	730.5 ± 15.94	758.3 ± 26.38	728.4 ± 33.23

standard deviation of the bending strength, and was shown in the figure. The figure also shows the bending strength of the multiple-indentation cracks (half-black

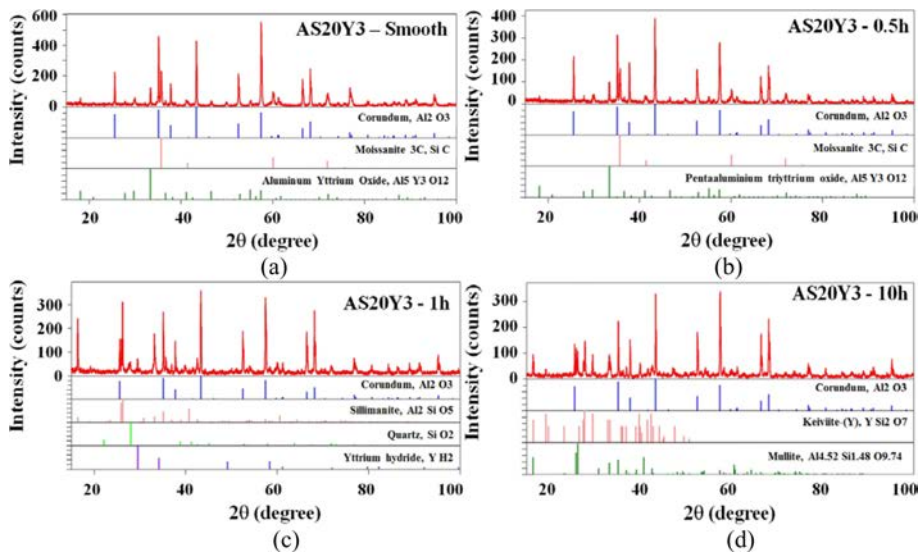


Fig. 15. XRD analysis according to healing time in AS20Y3. (a) 0 hr, (b) 0.5 hr, (c) 1 hr, (d) 10 hr.

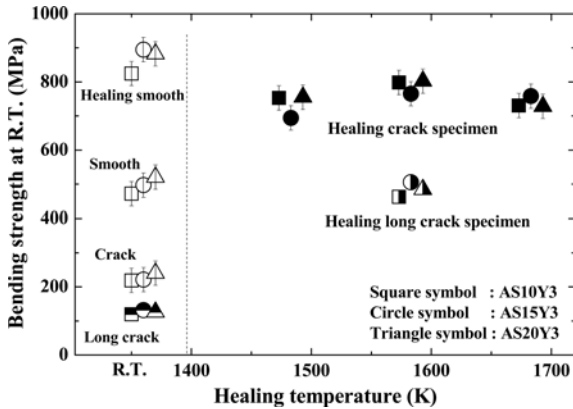


Fig. 16. Comparison for bending strength before and after healing.

symbols) for a comparison with the bending strength of a single indentation crack (white symbol, black symbol).

The square symbols (\square , \blacksquare) are the bending strengths that were obtained for the AS10Y3 specimen. The smooth specimen showed 472 MPa, but the crack specimen of the Vickers-indentation load of 19.6 N showed 219 MPa, which is approximately 46% of that of the smooth specimen. However, the healing smooth specimen showed 825 MPa, which is approximately 75% higher than that of the smooth specimen. Alternatively, the healing crack specimen showed strengths of 753, 798, and 731 MPa at 1473, 1573, and 1673 K, respectively, and these are 60, 69, and 55% higher than that of the smooth specimen, respectively.

The circular symbols (\circ , \bullet) are the bending strengths that were obtained for the AS15Y3 specimen. The smooth specimen showed 497 MPa, but the crack specimen of the Vickers-indentation load of 19.6 N showed 221 MPa, which is approximately 44% of the strength of the smooth specimen. However, the healing

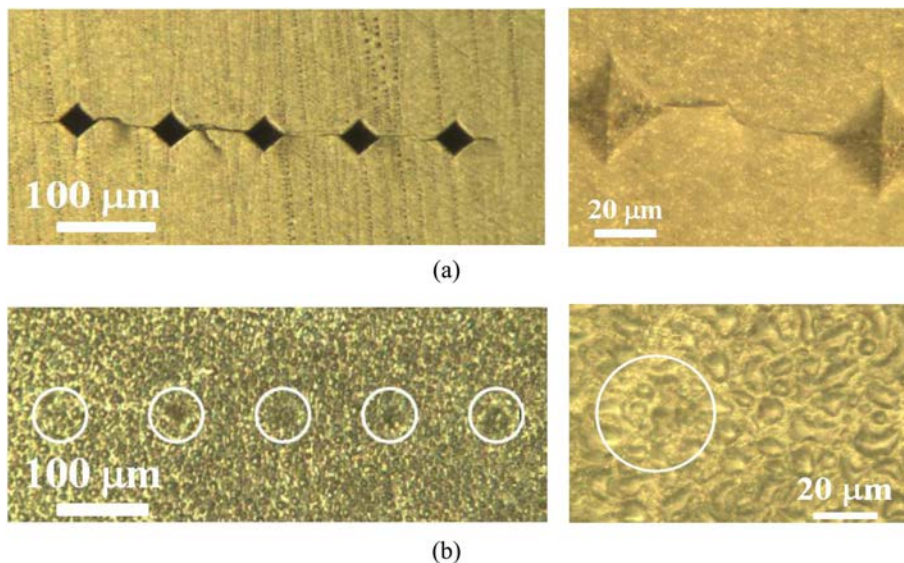


Fig. 17. SEM images of multiple indentation (a) before healing, (b) after healing.

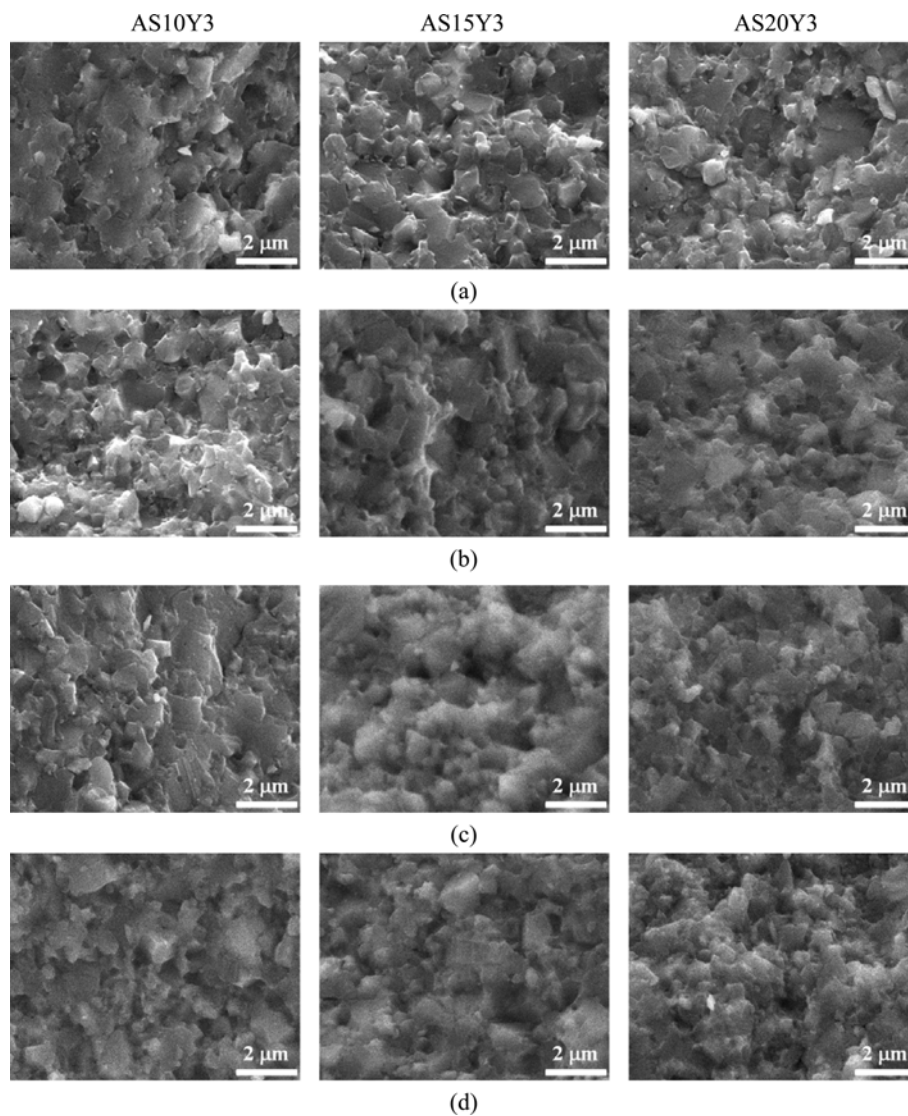


Fig. 18. SEM images of fracture surface. (a) Smooth specimen, (b) 1473 K heat treatment specimen, (c) 1573 K heat treatment specimen, (d) 1673 K heat treatment specimen.

smooth specimen showed 859 MPa, which is approximately 73% higher than that of the smooth specimen. Alternatively, the healing crack specimen showed strengths of 694, 766, and 758 MPa at 1473, 1573, and 1673 K, respectively, and these are 40, 54, and 53% higher than that of the smooth specimen, respectively.

The triangle symbols (\triangle , \blacktriangle) are the bending strengths that were obtained for the AS20Y3 specimen. The smooth specimen showed 520 MPa, but the crack specimen of the Vickers-indentation load of 19.6 N showed 240 MPa, which is approximately 46% of the strength of the smooth specimen. The healing smooth specimen, however, showed a strength of 883 MPa, which is approximately 70% higher than that of the smooth specimen. Alternatively, the healing crack specimen showed 755, 802, and 728 MPa at 1473, 1573, and 1673 K, respectively, and these are 45, 54, and 40% higher than that of the smooth specimen, respectively.

In Fig. 16, the bending strength of the crack specimen is approximately 55% smaller than that of the smooth specimen, and that of the healing smooth specimen is approximately 73% larger, regardless of the composition. Further, the healing crack specimen increased the bending strength by approximately 40-69% regardless of the temperature. Thus, the Al_2O_3 ceramic showed a significant increase of the bending strength due to the healing, regardless of the amount of added SiC and the heat-treatment temperature.

The bending strengths of the multiple-indentation long-crack specimens are 120, 132, and 126 MPa for the AS10Y3, AS15Y3, and AS20Y3 specimens, respectively, representing approximately 25% of the strength of each of the smooth specimens, which is much lower than those of the crack specimens. The bending strengths of the long-crack AS10Y3, AS15Y3 and AS20Y3 specimens that were heat-treated at 1573 K for 1 hr are 463, 506, and 484 MPa, respectively, thereby represent 98, 102,

and 93% for each of the smooth specimens that indicate an almost-recovered strength. The three specimens show similar healing properties, but in detail, it showed that the crack healing of the long-crack AS15Y3 specimen containing the 15 wt% SiC is slightly more effective.

The crack that was caused by the load of 19.6 N was healed by the heat treatment, and its bending strength is higher than that of the smooth specimen. The authors derived a healable crack-healing crack width using SiC composites, proving that even a long crack length can be healed by the maintenance of a healable crack width [8]. For this proof, the multiple-indentation long cracks of the 19.6 N load that were obtained from the AS20Y3 specimen are shown in Fig. 17, for which the crack healing was carried out at a healing temperature of 1573 K for 1 hr with the highest bending strength. Fig. 17(a) shows a multiple-indentation crack and an enlarged crack, and both of these cracks were connected to make a long crack; in 17(b), the appearance after the heat-treatment-derived crack healing is shown. In this figure, the cracks and indentations are completely healed.

Fig. 18 shows an SEM image of the fracture surface for all of the specimens. Regardless of the SiC composition, the structure of the heat-treated specimen is finer than that of the smooth specimen. In the case of the Y_2O_3 added specimens, the liquid phase was formed at a lower temperature and inhibited the growth of the crystal grains, leading to a fine microstructure. Further, the crystal grains were further sintered by the heat treatment, thereby increasing the strength.

Conclusions

This study evaluated the crack-healing characteristics of Al_2O_3 composites according to 10, 15, and 20 wt% concentrations of SiC. The long-crack healing strengths were also compared. The results are as follows:

(1) The cracks grew with the increasing of the indentation load regardless of the SiC contents. The crack lengths are the longest at the 10 wt% SiC, but those of the 15 wt% and 20 wt% SiC are nearly the same.

(2) The cracks of the three specimens were completely healed by the heat treatment including the complete healing of the long cracks. The amounts of Si and O in the crack parts of the crack specimens are small, but the amounts of Si and O in the crack-healing specimens increased. It is evident that the Si and O contributed to the crack healing.

(3) SiO_2 is dominant in the crack-healing behavior, but its amount changed with the SiC content. The 10 wt% SiC was detected as the Y_2O_3 - SiO_2 compound, the 15 wt% SiC was detected as the Al_2O_3 - SiO_2

compound, and the 20 wt% SiC was detected as both the Y_2O_3 - SiO_2 and Al_2O_3 - SiO_2 compounds. Therefore, even if the specimen component is the same, SiO_2 is present as a different type of compound depending on the mixing ratio.

(4) The bending strength of the crack specimen is approximately 60% smaller than that of the smooth specimen, but that of the healing smooth specimen is 70% larger. The crack-healing specimens are 61, 49, and 46% higher, respectively. The bending strength of the long-crack specimen is approximately 75% smaller than that of the smooth specimen, but the bending strength of the healing long-crack specimen is approximately 98% of that of the smooth specimen.

Acknowledgements

This work was supported by the Jungwon University Research Grant (2017-035).

References

1. K. Takahashi, M. Yokouchi, S.K. Lee, and K. Ando, *J. Am. Ceram. Soc.* 86 (2003) 2143-2147.
2. W. Nakao, M. Ono, S.K. Lee, K. Takahashi, and K. Ando, *J. Eur. Ceram. Soc.* 25 (2005) 3649-3655.
3. K. Takahashi, K. Uchiide, Y. Kimura, W. Nakao, and K. Ando, *J. Am. Ceram. Soc.* 90 (2007) 2159-2164.
4. K. Ando, T. Ikeda, S. Sato, F. Yao, and A. Kobayasi, *Fatigue Fract. Eng. Mater. Struct.* 21 (1998) 119-122.
5. S.K. Lee, W. Ishida, S.Y. Lee, K.W. Nam, and K. Ando, *J. Eur. Ceram. Soc.* 25 (2005) 569-576.
6. M.K. Kim, H.S. Kim, S.B. Kang, S.H. Ahn, and K.W. Nam, *Solid State Phenomena*, 124-126 (2007) 719-722.
7. K.W. Nam, M.K. Kim, S.W. Park, S.H. Ahn, and J.S. Kim, *Mater. Sci. Eng. A* 471 (2007) 102-105.
8. K.W. Nam, and J.S. Kim, *Mater. Sci. Eng. A* 527 (2010) 3236-3239.
9. K.W. Nam, J.S. Kim, and S.W. Park, *Mater. Sci. Eng. A* 527 (2010) 5400-5404.
10. K.W. Nam, J.S. Kim, and S.W. Park, *Int. J. Mod. Phys. B* 24 (2010) 2869-2874.
11. M. Ono, W. Nakao, K. Takahashi, M. Nakatani, and K. Ando, *Fatigue Fract. Engng Mater. Struct.* 30 (2006) 599-607.
12. T. Osada, W. Nakao, K. Takahashi, K. Ando, and S. Saito, *J. Eur. Ceram. Soc.* 27 (2007) 3261-3267.
13. M. Ono, W. Nakao, K. Takahashi, and K. Ando, *Fatigue Fract. Eng. Mater. Struct.* 30 (2007) 1140-1148.
14. C. Zdenek, F. Petr, K. Ando, and D. Ivo, *J. Eur. Ceram. Soc.* 28 (2008) 1073-1077.
15. K.W. Nam, *J. Ceram. Process. Res.* 11 (2010) 471-474.
16. K.W. Nam, J.S. Kim, and S.W. Park, *Int. J. Mod. Phys. B*, 24 (2010) 2869-2874.
17. K.W. Nam, and J.R. Hwang, *J. Mech. Sci. Tech.* 26 (2012) 2093-2096.
18. K.W. Nam, *Trans. Korean Soc. Mech. Eng. A* 40 (2016) 263-273.